Accurate and Efficient Spin-Spin Zero-Field Splitting Calculations for Extended Periodic Systems

T. Biktagirov, C. Braun, S. Neufeld, U. Gerstmann and W. G. Schmidt

Abstract Spin-spin zero-field splitting (ZFS) is a sensitive spectroscopic signature accessable by electron paramagnetic resonance. It is the key fingerprint used for the identification of high-spin defect centers in semiconducting host materials and for the characterization of their electronic structure. In recent years, much progress has been made in developing an efficient first-principles methodology for ZFS calculations that help in the interpretation of experimental data. Here we address the negatively charged nitrogen-vacancy center (NV^-) in diamond. It is used as a test system to explore the accuracy and efficiency of spin-spin zero-field splitting calculations on massively parallel computing systems.

1 Introduction

High-spin ($S \geq 1$) defect centers in semiconducting host materials are promising candidates for quantum information processing and sensing applications [1–3]. They rely on efficient detection and manipulation of their spin states. The first system for which such manipulations were realized is the negatively charged nitrogen-vacancy center (NV^-) in diamond. This defect exhibits a large ground-state transverse spin-relaxation time and optically induced spin polarization in a broad range of wavelengths at ambient conditions. Nowadays, there are other spin centers under investigation in diamond and silicon carbide (SiC) that possess similar spin properties, and the search for further structures continues.

The zero-field splitting (ZFS) accessable by electron-paramagnetic resonance (EPR) spectroscopy [4–6] is one of the key fingerprints used in the search for high-spin centers. It describes the interactions between the unpaired electrons in the absence of external magnetic fields and is extremely sensitive to the electronic structure and microscopic configuration of the defects. Within second order perturbation theory, the ZFS can be parametrised via the phenomenological spin-Hamiltonian

T. Biktagirov · C. Braun · S. Neufeld · U. Gerstmann · W. G. Schmidt (✉)
Lehrstuhl Für Theoretische Materialphysik Universität Paderborn,
33095 Paderborn, Germany
e-mail: W.G.Schmidt@upb.de

W. E. Nagel et al. (eds.), *High Performance Computing in Science and Engineering '18*, https://doi.org/10.1007/978-3-030-13325-2_8

and split into spin-spin and spin-orbit contributions [7]. For a number of important systems, such as spin centers in diamond and SiC, the spin-spin part is believed to be dominant [8, 9].

There exists a well-established framework for spin-spin ZFS calculation within all-electron density functional theory (DFT) for finite size systems [10–12]. It is frequently used for molecular systems. This methodology is, however, not directly applicable to extended periodic systems, due to unavoidable finite-size effects. This is in particular the case for defects with strongly delocalized spin density, typical for spin centers in semicoductors. While it is in principle possible to approximate the semiconductor host material by finite clusters [13, 14], the numerical convergence with respect to the cluster size is typically slow and requires extensive computational resources.

Therefore, the more suitable way is to adopt the supercell approach with explicitly imposed periodic boundary conditions. It relies on Bloch's theorem and involves Fourier transformation of the basic quantities into the reciprocal space. This strategy is routinely employed in computational materials science for the calculations of various properties, often in combination with pseudopotentials. The supercell approach can be effectively complemented with Blöchl's projector augmented wave (PAW) formalism [16] for EPR parameter calculations. In this method, all-electron wave functions are substituted by smooth pseudo-wave functions expanded in plane waves, while the true shape of the wave functions within the atomic core region is preserved. This allows for addressing all-electron properties with the efficiency of pseudopotential calculations.

The gauge-including extension of the projector augmented wave formalism (GIPAW) [17], which ensures the translational invariance of the wave-functions in external magnetic fields, has already proven highly successful for the ab initio calculation of EPR parameters. Recently, we presented an implementation of the spin-spin contribution to ZFS within the PAW formalism [18] that allows for their efficient calculation using periodic boundary conditions. The comparison with all-electron calculations, shown in Fig. 1 for a series of high-spin defects in hydrogen-terminated

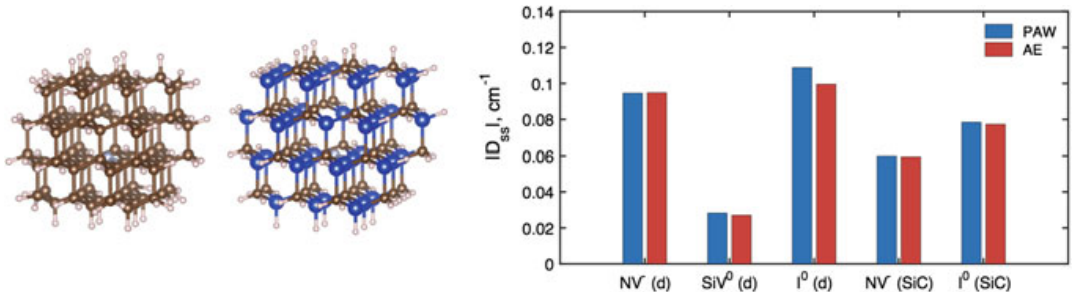

Fig. 1 Comparison of the spin-spin ZFS calculated with the present `GIPAW` implementation using the `Quantum ESPRESSO` code (*blue*) with results obtained using the all-electron (AE) approach implemented in the `ORCA` package [15] (*red*) for the same hydrogen-terminated clusters cut from optimized supercells (*left*). Shown are data for the nitrogen-vacancy center (NV^-) in diamond and SiC, the neutral silicon-vacancy (SiV^0) center in diamond, and the neutral carbon self-interstitial (I^0) in diamond and SiC

clusters of diamond and cubic SiC, demonstrates that this implementation reaches chemical accuracy of the calculated spin-spin ZFS.

The successful application of the implemented algorithms requires the control over all technical factors that affect the precision of the calculated ZFS. The spurious dipole-dipole interaction between the periodic replicas and the strain-induced redistribution of the spin density within the supercell are among the main sources of possible errors in this context. In principle, both factors are related to the size of the supercell used for calculations. This relation is obvious for dipole-dipole interaction, since it explicitly depends on spatial separation between the periodic copies of the defect. Furthermore, the calculated ZFS of the defect can sense local strain fields produced by the replicas, which should vanish upon increasing the supercell size. In either case, the results for larger supercells are expected to be more reliable. The computational costs, however, scale unfavorably with the size of the supercell.

Therefore, in this report we investigate how the accuracy of spin-spin ZFS calculations depends on the supercell size. The negatively charged nitrogen-vacancy center (NV^-) in diamond is chosen as an ideal candidate for the numerical tests. Particular emphasis is placed (i) on the possibility to obtain sufficiently accurate results with smaller cells upon assuring the convergence with respect to the Brillouin zone sampling in the reciprocal space (i.e. the number of used k-points) and (ii) on the performance of our implementation on the HLRS computing resources.

We mention that a similar study for spin centers in SiC was recently reported in Ref. [19]. There other essential spectroscopic fingerprints, i.e., the zero-phonon line and the hyperfine coupling were explored. We believe that the present results are a valuable contribution to the understanding and optimization of computational schemes for the comprehensive ab initio characterization of spin centers.

2 Methodology

The algorithms implemented in the `GIPAW` module of the `Quantum ESPRESSO` software [20, 21] are based on the the theoretical framework thoroughly described in Ref. [18]. Here, we only provide a brief outline of the methods with an extra focus put on technical details of their implementation.

Conventionally, the spin-spin ZFS is defined in terms of a phenomenological spin Hamiltonian [22] as a symmetric 3×3 tensor $\mathbf{D}$:

$$\hat{H}_{\mathrm{SS}} = \frac{\alpha^2}{2} \sum_{m,n} \left[\frac{\hat{\mathbf{s}}_m \cdot \hat{\mathbf{s}}_n}{r_{mn}^3} - 3 \frac{(\hat{\mathbf{s}}_m \cdot \mathbf{r}_{mn})(\hat{\mathbf{s}}_n \cdot \mathbf{r}_{mn})}{r_{mn}^5} \right] = \hat{\mathbf{S}} \cdot \mathbf{D} \cdot \hat{\mathbf{S}} \,. \tag{1}$$

In Eq. (1), α is the fine-structure constant, $\mathbf{r}_{mn}$ is the vector between electrons m and n, and $\hat{\mathbf{S}}$ is the total effective spin of the system. To further address the $\mathbf{D}$ tensor from first-principles calculations, it is convenient to reformulate it by separating the spin and spatial degrees of freedom ($a, b = x, y, z$) [23]:

$$D_{ab} = \sum_{m,n} f_m f_n \sigma_{mn} D_{ab,mn} \,, \tag{2}$$

where f_m, f_n are the occupations of the orbitals m and n, and σ_{mn} originates from the matrix elements of spin-operators: $\sigma_{mn} = 1$ for parallel spins and $\sigma_{mn} = -1$ in case of antiparallel spins. In Eq. (2) the space-dependent part of the spin-spin ZFS contribution from two orbitals, m and n, is given by McWeeny and Mizuno [23]

$$\begin{aligned} D_{ab,mn} = \frac{\alpha^2}{4S(2S-1)} \int d^3\mathbf{r} d^3\mathbf{r}' \frac{|\mathbf{r}-\mathbf{r}'|^2 \delta_{ab} - 3(\mathbf{r}-\mathbf{r}')_a (\mathbf{r}-\mathbf{r}')_b}{|\mathbf{r}-\mathbf{r}'|^5} \\ \times \left[n_{mm}(\mathbf{r}) n^*_{nn}(\mathbf{r}') - n_{mn}(\mathbf{r}) n^*_{mn}(\mathbf{r}') \right] , \end{aligned} \tag{3}$$

which consists of Coulomb-like and exchange-like contributions. In the above expression we define the charge density, $n_{mn}(\mathbf{r}) = \psi^*_m(\mathbf{r})\psi_n(\mathbf{r})$, from the space distribution of the spin orbitals.

In case of all-electron calculations, the densities $n_{mn}(\mathbf{r})$ are readily available from the self-consistent field (SCF) calculations. However, when the pseudopotential approach is utilized, the resulting charge densities are devoid of important details about the true shape of the spin orbitals in the core region. As already mentioned in the introduction, this problem can be circumvented within the PAW framework. Here, the two-electron density is presented by a superposition

$$n_{mn}(\mathbf{r}) = \tilde{n}_{mn}(\mathbf{r}) + \sum_R (n^R_{mn}(\mathbf{r}) - \tilde{n}^R_{mn}(\mathbf{r})) \tag{4}$$

of the smooth pseudo-density $\tilde{n}_{mn}(\mathbf{r}) = \langle \tilde{\Psi}_m | \mathbf{r} \rangle \langle \mathbf{r} | \tilde{\Psi}_n \rangle$ treated on a plane-wave grid, and the difference between on-site expansions of the all-electron density n^R and the pseudo-density $\tilde{n}^R$ defined on a radial grid within the augmentation sphere around an atomic site R.

As justified in Ref. [18] for norm-conserving pseudopotentials, the spin-spin ZFS also can be constructed in a form of three non-interacting contributions,

$$D_{ab} = \tilde{D}_{ab} + \sum_R \left[D^R_{ab} - \tilde{D}^R_{ab} \right] = \tilde{D}_{ab} + \Delta D_{ab} \,, \tag{5}$$

where the sum ΔD_{ab} of the on-site terms constitutes the essence of the PAW reconstruction.

Thereby the treatment of ΔD_{ab} is based on evaluation of the following four-partial-wave two-electron integral [18],

$$\begin{aligned} W^R_{ab,ijkl} = \int\limits_{\Omega_R} d^3\mathbf{r} d^3\mathbf{r}' \langle \phi_i | \mathbf{r} \rangle \langle \mathbf{r} | \phi_j \rangle \langle \phi_l | \mathbf{r}' \rangle \langle \mathbf{r}' | \phi_k \rangle \\ \times \left\{ (\frac{1}{3} \delta_{ab} \nabla^2 - \partial_a \partial_b)_{r'} \frac{1}{|\mathbf{r}-\mathbf{r}'|} \right\} , \end{aligned} \tag{6}$$

where the index $i \in R$ refers to angular momentum quantum numbers l_i and m_i for the atom R. The all-electron partial wave ϕ_i is a solution of the radial Schrödinger (or Dirac) equation for the reference atom. The pseudo partial wave $\tilde{\phi}_i$ is equivalent to ϕ_i outside the augmentation sphere. In $W^R_{ab,ijkl}$, angular integration can be further performed analytically making the evaluation of ΔD_{ab} computationally very efficient.

The implementation of the plane-wave pseudo-density contribution, $\tilde{D}_{ab}$, is based on the work by Rayson and Briddon [24, 25], who formulate it in reciprocal space as

$$\tilde{D}_{ab,mn} = \frac{\alpha^2 \Omega \pi}{S(2S-1)} \sum_{\mathbf{G}} \left(\frac{G_a G_b}{G^2} - \frac{\delta_{ab}}{3} \right) \left[\tilde{n}_{mm}(\mathbf{G}) \tilde{n}_{nn}(-\mathbf{G}) - |\tilde{n}_{mn}(\mathbf{G})|^2 \right]. \quad (7)$$

In the above expression, $\tilde{n}_{mm}(\mathbf{G})$ and $\tilde{n}_{nn}(-\mathbf{G})$ are the Fourier coefficients of the two-electron densities at the points $\mathbf{G}$ and $-\mathbf{G}$, and Ω is the volume of the unit cell. Note that Eq. (7) corresponds to the situation where the Brillouin zone is sampled with only one single k point. It can be generalized to a denser sampling by substituting $\mathbf{G}$ by $\mathbf{G} + \mathbf{k}$, where the summation is to be made over $\mathbf{G}$ as well as $\mathbf{k}$.

In practice, numerical evaluation of $\tilde{D}_{ab,mn}$ involves a two-step procedure. First, the pseudo-wave functions are Fourier transformed to the plane-wave grid in real space, where the two-electron densities are subsequently constructed. Then the densities are transferred again to the reciprocal space, and the summation in Eq. (7) is computed. The procedure has to be carried out for each orbital pair m and n. This makes $\tilde{D}_{ab,mn}$ the computationally most demanding term in Eq. (5). To assure reasonable efficiency of the implementation, our code was thus designed to support parallelization with respect to the plane-wave coefficients. This is achieved by redistributing the coefficients across the processors in such a way that for each processor both $\tilde{n}_{mm}(\mathbf{G})$ and the corresponding $\tilde{n}_{nn}(-\mathbf{G})$ are addressable [(cf. Eq. (7)].

The overall procedure of computing D_{ab} is thus as follows. At the first step, we determine the electronic ground state in the `PWSCF` module of the `Quantum ESPRESSO` software. We restrict ourselves to norm-conserving pseudopotentials (generated with the Troullier-Martins approach [26]) and the PBE exchange-correlation functional [27] in the numerical tests presented below. The convergence criterion for the geometry optimization was set to 10^{-4} Ry/Bohr. At the next step, the numerically converged ground-state orbitals are taken over by the `GIPAW` module, where the $\tilde{D}_{ab}$ and ΔD_{ab} contributions are evaluated separately.

3 Results

For the numerical tests, we have chosen the NV^- defect in diamond (see Fig. 2). In this so-called color center, the nitrogen impurity occupies a substitutional site neighboring the carbon vacancy. The nitrogen-vacancy pair is formed in such a way

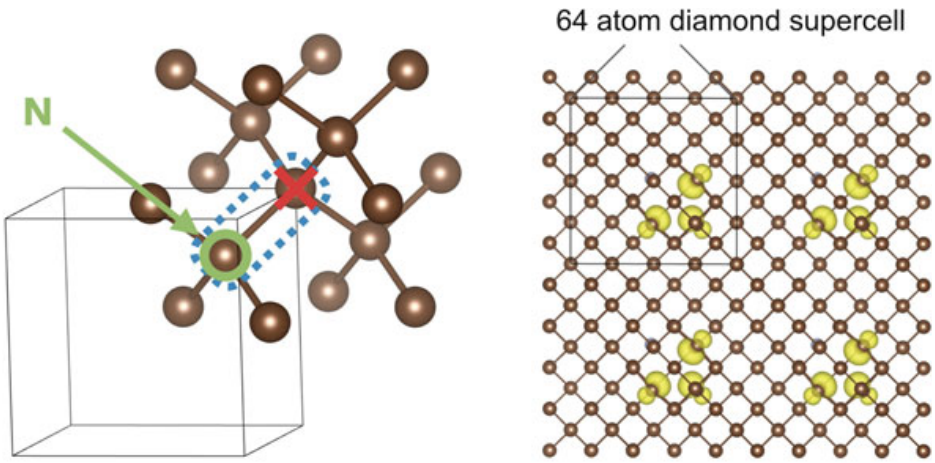

Fig. 2 Schematics of the microscopic model of the NV^- center in diamond (*left*) and an illustration of the 64-atom diamond supercell containing the center (*right*). Yellow isosurfaces represent the spin-density distribution of the defect over the three carbon dangling bonds surrounding the vacancy

that the symmetry axis of the complex coincides with the [111] axis of the crystal. At the ground state ($^3A_2$, $S = 1$) the center manifests C_{3v} point group symmetry with the spin density mostly localized on the three carbon dangling bonds surrounding the vacancy. Its ZFS (of about 2.88 GHz [28]) is supposed to be almost entirely caused by the spin-spin contribution [8], which makes it a perfect choice for the current study.

We begin by incorporating NV^- into a series of cubic diamond supercells with increasing size. It is expected that the small supercells are most affected by the spurious influence from the periodic replicas of the defect. The ideal case scenario would imply isolating a defect center by using as large supercells as possible within the available computational resources. However, also in the experiment the color center is never entirely isolated, because of unavoidable presence of different kinds of other defects and impurities in the host material [29]. Therefore, the essential question is, whether it is possible to achieve *sufficient* accuracy of the calculated spin-spin ZFS without pushing the size of supercell beyond the limits of a reasonable computational cost.

Thus, for each of the considered supercells we had to assure tight convergence of the results. In particular, we study the convergence behaviour of the ZFS with respect to the level of Brillouin zone sampling (i.e. the number of k points) used in the SCF cycle. For another convergence parameter, the plane-wave cutoff, the same (and sufficiently large [18]) value of 50 Ry was used for all of the supercell sizes. Therefore, its influence is not further discussed.

The convergence of D_{SS} with respect to the dimensions of a Monkhorst-Pack [30] k-point grid is illustrated in Fig. 3 for different supercell sizes. The first conclusion is that a single k point for Brillouin zone sampling is in general not sufficient. Aside from that, the smaller supercells demonstrate slower convergence, and require denser k-point grids. This becomes particularly obvious in the extreme case of a 8-atom supercell. Here, the calculated D_{SS} value is converged within a 10×10^{-4} cm^{-1}

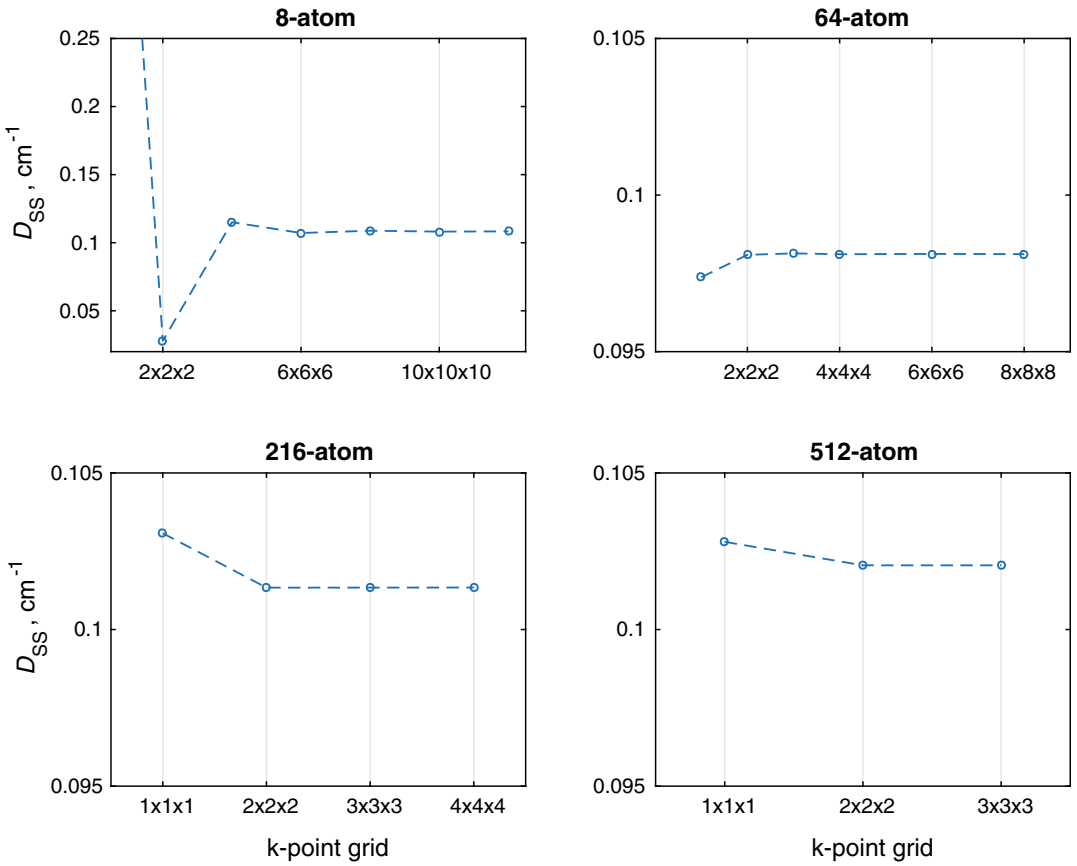

Fig. 3 Spin-spin ZFS (D_{SS}) calculated for the NV^- center in diamond supercells of varying size: Convergence behavior with respect to the Brillouin zone sampling, i.e. the number of k-points generated according to the Monkhorst-Pack scheme [30]

window only for k-point grids as large as at least $6 \times 6 \times 6$. Of course, such a small supercell is considered here only for the purpose of numerical exercise and should not be used in practice, when agreement with experimental data is desired.

With this being said, we can then carry out a comparative analysis of the converged results obtained with different supercell sizes. The major conclusion which can be derived from the data presented in Fig. 4 is that even comparably small supercells can provide results within a reasonable level of error, provided k-point convergence is ensured. Surprisingly, even the D_{SS} value calculated for the 8-atom supercell is not too far off. However, we cannot exclude that this is due to fortuitous error cancellation. The 216-atom supercell provides a much more reasonable choice, and the corresponding D_{SS} deviates by only 2% from the value obtained for the largest system considered here.

These results provide an obvious guideline for practical calculation of spin-spin ZFS: One strategy is to use a reasonably small supercell with sufficiently dense k-point mesh. Alternatively, the supercell size might be increased and the Brillouin zone sampling restricted to a single k-point. The latter strategy provides more accurate D values and is mandatory for spin centers that show very small ZFS, which is easily

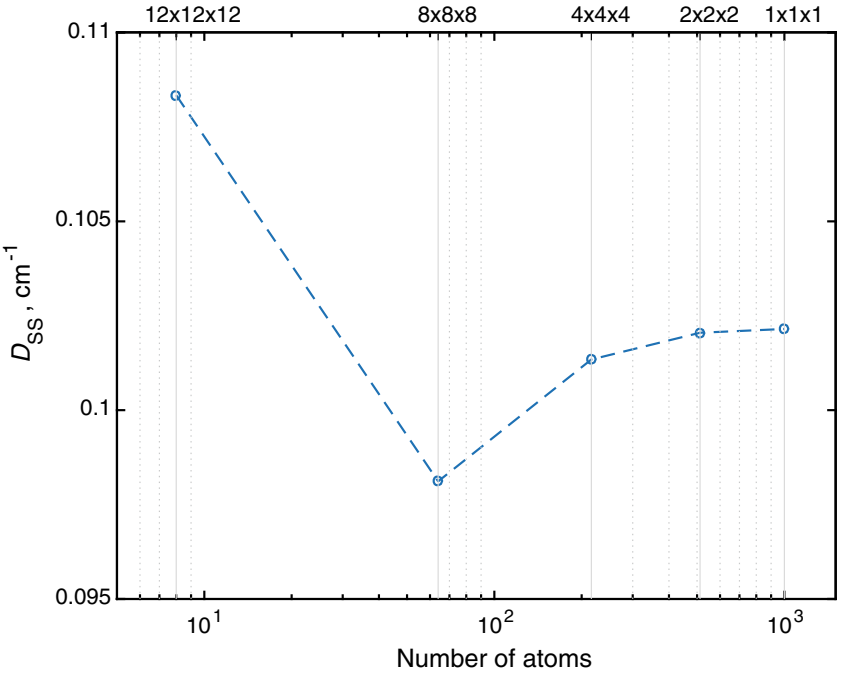

Fig. 4 Dependence of the spin-spin ZFS (D_{SS}) calculated for the NV^- center in diamond on the supercell size. For each supercell, the presented value was previously converged with respect to the number of k-points (the required dimensions of the k-point grid are shown on the topmost horizontal axis.)

masked by numerical noise. However, the usage of large unit cells is computationally expensive.

Therefore, an important question is how well do the underlying algorithms perform on massively parallel systems such as the Cray XC40 (Hazel Hen) for a relatively large supercells. As mentioned above in the Methodology section, our implementation supports parallelization over plane-wave expansion coefficients (whose number increases upon increasing of the supercell size). This leads to efficient speed up of the calculations and is expected to provide efficient scaling. Figure 5 illustrates the performance of the Cray XC40 for spin-spin ZFS calculation for NV^- in a 216-atom supercell (with the plane-wave cutoff increased up to 100 Ry). It can be seen that the parallelization which distributes the plane-wave expansion coefficients indeed leads to an appreciable saving of computation time with increasing number of cores. However, the speed up saturates already for a few hundred cores. Therefore it is essential to improve the scalability further. This is presently done by exploring the parallelization over **k** points as well as over electronic states. However, as in case of exact exchange functionals [31], the "sum-over-pairs of states" nature of the ZFS hinders their straightforward implementation.

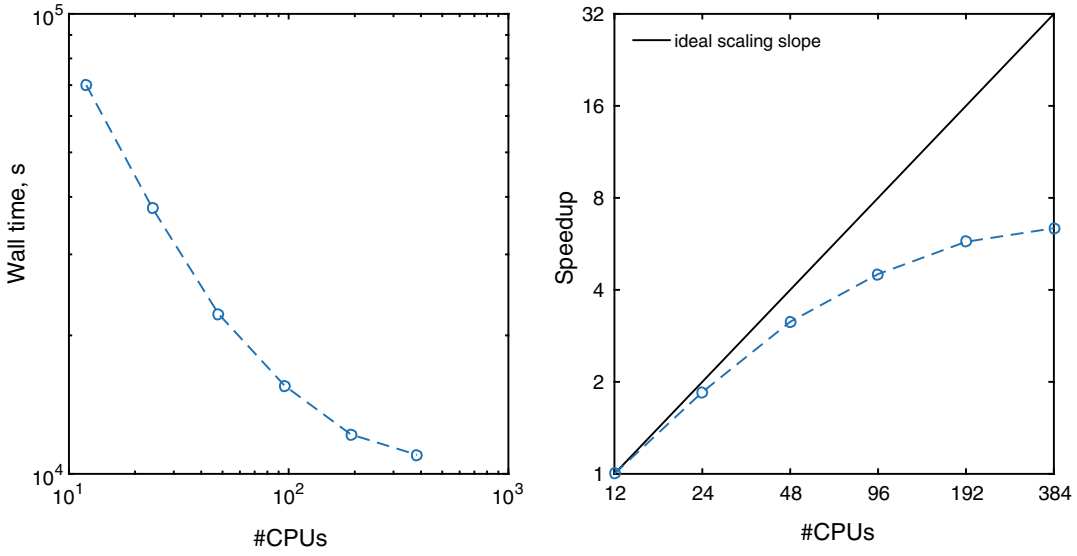

Fig. 5 Scaling of spin-spin ZFS calculation for the NV^- center in 216-atom diamond supercell with high plane-wave cutoff of 100 Ry on the HLRS Cray XC40. MPI parallelization is restricted to the plane waves

4 Conclusions

To summarize, in the present report we addressed the accuracy and performance of our recently developed MPI-based implementation for DFT based calculations of spin-spin ZFS with periodic boundary condition. The zero-field splitting is a sensitive spectroscopic signature, and its ab initio evaluation requires a high level of precision. The number of k points used for the Brillouin zone sampling is found to have a crucial influence on the calculated D values. Provided the k-point grid is chosen sufficiently dense, the ZFS calculations may be accurate even for relatively small supercells. In case of the NV^- center in diamond considered here, cubic 216 and 512 atom supercells appear to be appropriate for routine calculations. On the other hand, when very high precision is required (e.g. to identify defects with extremely small D values) larger unit cells may be necessary. This requires the usage of massively-parallel computing systems, such as the Cray XC40. However, the scalability of our code still needs to be improved.

Acknowledgements The Deutsche Forschungsgemeinschaft is acknowledged for financial support (SPP1601, FOR1700 and SFB TRR 142). We thank the Höchstleistungs-Rechenzentrum Stuttgart (HLRS) and the Paderborn Center for Parallel Computing (PC^2) for grants of high-performance computer time. Images of molecular structures were prepared using VESTA [32].

References

1. D. DiVincenzo, Nat. Mater. **9**, 468–469 (2010)
2. D.D. Awschalom, L.C. Bassett, A.S. Dzurak, E.L. Hu, J.R. Petta, Science **339**, 1174–1179 (2013)
3. H.J. Mamin, M. Kim, M.H. Sherwood, C.T. Rettner, K. Ohno, D.D. Awschalom, D. Rugar, Science **339**, 557–560 (2013)
4. H.J. Von Bardeleben, J.L. Cantin, E. Rauls, U. Gerstmann, Phys. Rev. B **92**, 064104 (2015)
5. V.A. Soltamov, B.V. Yavkin, D.O. Tolmachev, R.A. Babunts, A.G. Badalyan, V.Yu. Davydov, E.N. Mokhov, I.I. Proskuryakov, S.B. Orlinskii, P.G. Baranov, Phys. Rev. Lett. **115**, 247602 (2015)
6. A. Csóré, H.J. von Bardeleben, J.L. Cantin, A. Gali, Phys. Rev. B **96**, 085204 (2017)
7. J.E. Harriman, *Theoretical Foundations of Electron Spin Resonance* (Academic press, New York, 1978)
8. V. Ivády, T. Simon, J.R. Maze, I.A. Abrikosov, A. Gali, Phys. Rev. B **90**, 235205 (2014)
9. H.J. Von Bardeleben, J.L. Cantin, A. Csóré, A. Gali, E. Rauls, U. Gerstmann, Phys. Rev. B **94**, 121202 (2016)
10. F. Neese, J. Am. Chem. Soc. **128**, 10213–10222 (2006)
11. S. Sinnecker, F. Neese, J. Phys. Chem. A **110**, 12267–12275 (2006)
12. F. Neese, J. Chem. Phys. **127**, 164112 (2007)
13. T.T. Petrenko, T.L. Petrenko, V. Ya Bratus, J. Phys. Condens. Matter **14**, 12433 (2002)
14. A. Komarovskikh, A. Dmitriev, V. Nadolinny, Y. Palyanov, Diam. Relat. Mater. **76**, 86–89 (2017)
15. F. Neese, Wiley Interdiscip. Rev. Comput. Mol. Sci. **2**, 73–78 (2012)
16. P.E. Blöchl, Phys. Rev. B **50**, 17953 (1994)
17. C.J. Pickard, F. Mauri, Phys. Rev. B **63**, 245101 (2001)
18. T. Biktagirov, W.G. Schmidt, U. Gerstmann Phys. Rev. B **97**, 115135 (2018)
19. J. Davidsson, V. Ivdy, R. Armiento, N.T. Son, A. Gali, I.A. Abrikosov, New J. Phys. **20**, 023035 (2018)
20. P. Giannozzi, O. Andreussi, T. Brumme et al., J. Phys. Condens. Matter **29**, 465901 (2017)
21. P. Giannozzi, S. Baroni, N. Bonini, M. Calandra et al., J. Phys. Condens. Matter **21**, 395502 (2009)
22. R. McWeeny, *Methods of Molecular Quantum Mechanics* (Academic press, 1992)
23. R. McWeeny, Y. Mizuno, in *Proceedings of the Royal Society of London A: Mathematical, Physical and Engineering Sciences*, vol. 259 (The Royal Society, 1961), pp. 554–577
24. M.J. Rayson, P.R. Briddon, Phys. Rev. B **77**, 035119 (2008)
25. Z. Bodrog, A. Gali, J. Phys. Condens. Matter **26**, 015305 (2013)
26. N. Troullier, J.L. Martins, Phys. Rev. B **43**, 1993 (1991)
27. J.P. Perdew, K. Burke, M. Ernzerhof, Phys. Rev. Lett. **77**, 3865 (1996)
28. J. Loubser, J. van Wyk, Rep. Prog. Phys. **41**, 1201 (1978)
29. T. Biktagirov, A.N. Smirnov, V.Yu. Davydov, M.W. Doherty, A. Alkauskas, B.C. Gibson, V.A. Soltamov, Phys. Rev. B **96**, 075205 (2017)
30. H.J. Monkhorst, J.D. Pack, Phys. Rev. B **13**, 5188 (1976)
31. T.A. Barnes, T. Kurth, P. Carrier, N. Wichmann, D. Prendergast, P.R. Kent, J. Deslippe, Comput. Phys. Commun. **214**, 52 (2017)
32. K. Momma, F. Izumi, J. Appl. Crystallogr. **44**, 1272 (2011)